

Relative Orbital Elements Formulation Based upon the Clohessy-Wiltshire Equations

Thomas A. Lovell · David A. Spencer

Published online: 10 February 2015
© American Astronautical Society 2015

Abstract For on-orbit applications where two or more spacecraft are flying in close proximity, it is often convenient to apply the Clohessy-Wiltshire differential relative motion equations in order to calculate the relative motion of a deputy spacecraft about a chief spacecraft that is assumed to be in a circular orbit. Under these assumptions, the solutions to the Clohessy-Wiltshire equations can be re-parameterized as a set of relative orbital elements that fully characterize the relative motion of the deputy about the chief. In contrast to the Cartesian relative position and velocity states, relative orbital elements provide a clear geometric interpretation of the relative motion and yield an intuitive understanding of how the unforced relative motion will evolve with time. In this paper, the derivation of relative orbital elements is given, and the transformation between relative orbital elements and Cartesian state elements expressed in the local-vertical, local-horizontal frame is provided. The evolution of relative orbital elements with time is evaluated, and characteristics of the unforced motion in terms of relative orbital elements are described.

Keywords Orbital mechanics · Relative motion · Proximity operations

Thomas A. Lovell is a Research Aerospace Engineer, Space Vehicles Directorate, Air Force Research Laboratory; Associate Fellow, AIAA; Senior Member, AAS.

David A. Spencer is a Professor of the Practice, Guggenheim School of Aerospace Engineering, Georgia Institute of Technology, Atlanta, GA 30332-0150, Associate Fellow, AIAA, Member AAS.

T. A. Lovell
Air Force Research Laboratory, Kirtland AFB, Albuquerque, NM 87117, USA

D. A. Spencer (✉)
Georgia Institute of Technology, Atlanta, GA 30332, USA
e-mail: david.spencer@aerospace.gatech.edu

Nomenclature

- a_r = semimajor axis of the instantaneous relative ellipse
 a_{T_x} = radial component of acceleration resulting from external forces
 a_{T_y} = along-track component of acceleration resulting from external forces
 a_{T_z} = cross-track component of acceleration resulting from external forces
 A_x = amplitude of the motion in the LVLH radial direction
 A_y = amplitude of the motion in the LVLH along-track direction
 A_z = amplitude of the motion in the LVLH cross-track direction
 E_r = relative eccentric anomaly
 i_r = relative inclination
 n = mean motion of the chief's orbit
 \bar{n}_r = vector normal to the instantaneous relative orbit
 \hat{n}_r = unit vector normal to the instantaneous relative orbit
 \mathbf{r} = magnitude of deputy position vector with respect to center of central body
 $\bar{\mathbf{r}}$ = deputy position vector with respect to center of central body
 $\bar{\mathbf{r}}^C$ = chief position vector with respect to center of central body
 $\bar{\mathbf{r}}_1$ = position vector from the instantaneous center of motion to the point where $E_r = 0$
 $\bar{\mathbf{r}}_2$ = position vector from the instantaneous center of motion to the point where $E_r = \pi/2$
 t = time
 x = relative position vector component in LVLH radial direction
 \dot{x} = derivative with respect to time of relative position vector component in LVLH radial direction, taken in LVLH frame
 \ddot{x} = second derivative with respect to time of relative position vector component in LVLH radial direction, taken in LVLH frame
 \hat{x} = LVLH coordinate unit vector in radial direction
 x_r = radial coordinate of instantaneous center of motion
 x_q = radial coordinate of point Q on circle that circumscribes instantaneous relative orbit ellipse
 y = relative position vector component in LVLH along-track direction
 \dot{y} = derivative with respect to time of relative position vector component in LVLH along-track direction, taken in LVLH frame
 \ddot{y} = second derivative with respect to time of relative position vector component in LVLH along-track direction, taken in LVLH frame
 \hat{y} = LVLH coordinate unit vector in along-track direction
 y_r = along-track coordinate of instantaneous center of motion
 y_q = along-track coordinate of point Q on circle that circumscribes instantaneous relative orbit ellipse
 y_s = secular drift in LVLH along-track direction
 \dot{y}_s = secular drift rate in LVLH along-track direction
 z = relative position vector component in LVLH cross-track direction
 \dot{z} = derivative with respect to time of relative position vector component in LVLH cross-track direction, taken in LVLH frame

- \ddot{z} = second derivative with respect to time of relative position vector component in LVLH cross-track direction, taken in LVLH frame
 \hat{z} = LVLH coordinate unit vector in cross-track direction
 γ = phase difference between relative eccentric anomaly and cross-track motion phase angle
 μ = gravitational parameter of central body
 v_r = relative true anomaly
 $\bar{\rho}$ = deputy relative position vector with respect to chief
 $\bar{\rho}^{I/C}$ = position vector from LVLH origin to instantaneous center of relative motion
 $\bar{\rho}_1$ = position vector from LVLH origin to location on relative orbit where $E_r = 0$
 $\bar{\rho}_2$ = position vector from LVLH origin to location on relative orbit where $E_r = \pi/2$
 ψ = cross-track motion phase angle
 0 = subscript indicating initial condition

Introduction

The close proximity flight of two or more spacecraft in orbit has been increasingly utilized in order to achieve mission objectives spanning on-orbit inspection [1], formation flight [2, 3], space station resupply [4], and satellite servicing [5, 6], for commercial and defense applications. The increasing prevalence of nano- and micro-spacecraft and emerging architectures including fractionated spacecraft have added to the priority of robust close proximity trajectory design and control [7, 8]. While the mission objectives related to close proximity operations are diverse, there exists a set of relative trajectory control behaviors that are common to most close proximity mission architectures, including rendezvous and station-keeping. Cooperative formation missions often must satisfy a stringent requirement on the relative spacing of the satellites in the cluster. For on-orbit inspection applications, circumnavigation of the targeted space object may be desired. For satellite servicing or resupply missions, close approach and mating must occur. Underlying all of these behaviors is the requirement to maintain safe relative trajectories, where collision avoidance is assured [10–13].

For the above applications, the relative motion between spacecraft is of interest. Analytical models for relative motion appeared as early as 1878 [14], while in more recent history, the past five decades have seen a wealth of literature on the subject. Two of the most widely accepted models developed during that era are that of Tschauner and Hempel [15] and that of Clohessy and Wiltshire [16]. Both models linearize the motion of a “deputy” spacecraft about a “chief” spacecraft, with the latter model assuming a circular chief orbit.

In addition to possessing an analytical model, a clear understanding of the physical motion between close proximity spacecraft on orbit is critical to the design of safe, robust mission plans [17]. Previous works have identified constants of the relative motion. Schaub and Junkins [18] and Vallado [19] defined scalar offsets in the orbit radial and along-track directions, representing the instantaneous center of the

motion in the plane of the chief's inertial orbit. Vallado described the amplitude of the oscillatory motion in the chief's orbital plane, and he defined a constant that is consistent with the amplitude of the motion in the cross-track direction. Kaplan defined a relative eccentricity parameter of the chase orbit [20]. Gustafson and Kriegsmann utilized dynamics of the relative motion to develop parametric equations for automated station-keeping in Earth orbit [21].

Previous works have defined and utilized geometric parameterizations of relative motion. One such common formulation is to represent the differences in classical orbital elements between the deputy and chief as the relative states [18, 22]. A relative parameter set that has seen extensive mission application is that developed by D'Amico and Montenbruck [23]. These particular parameters consist of either orbital element differences between the deputy and chief, or nonlinear combinations thereof. Ref. [24] showed that these parameters match the integration constants of the Clohessy-Wiltshire equations. This parameter set has been applied to several close-proximity missions, most notably PRISMA [25, 26]. Han and Yin [27] put forward a set of geometric relative coordinates very similar to those of Ref. [14], and demonstrate their use for elliptical chief relative motion.

This investigation advances the development of a parameterization called relative orbital elements (ROEs) for close proximity mission planning. ROEs represent a direct re-parameterization of the solutions to the Clohessy-Wiltshire equations. Lovell, Tragesser and Tollefson initially formulated ROEs in 2004 [28, 29], defining six elements that fully characterize the Clohessy-Wiltshire relative motion, and establishing the transformation between ROEs and Cartesian coordinates in the local vertical-local horizontal (LVLH) coordinate frame. They also showed the effect of one or more instantaneous maneuvers on ROEs, and developed a multiple-impulse guidance methodology for relative trajectory control. These advancements provide a useful framework for relative orbit mission planning. Analogous to classical orbital elements, ROEs provide a geometric interpretation of the relative motion of a deputy spacecraft with respect to a chief spacecraft that is in a circular orbit. ROEs allow the characterization of the deputy spacecraft relative motion in an unforced (free-motion) trajectory, and provide a direct visualization of the effects of maneuvers on the relative motion geometry.

Since the introduction of ROEs in 2004, the formulation has been used for the development of several analytical guidance strategies. Bevilacqua and Lovell [30] developed relative motion guidance solutions applying continuous, on-off thrust, and utilizing ROEs as a geometrical representation of the dynamics. Phillips [31] utilized ROEs for determination of satellite collision probability. Aubin [32] employed ROEs to generate solution vectors for a particle swarm evolutionary algorithm. Schwartz et al [33, 34] developed an ROE-based controller for station-keeping of a cluster of spacecraft as part of the DARPA System F6 flight program. The Prox-1 small satellite mission will apply impulsive control strategies based upon ROEs to implement formation flight and circumnavigation maneuvers [35].

This article formally documents the derivation of the ROE parameterization. Through this work, a geometric interpretation of the angular ROEs is provided, leading to a strong analogy between ROEs and classical orbital elements. Additional parameters related to ROEs are described, including the newly defined parameters

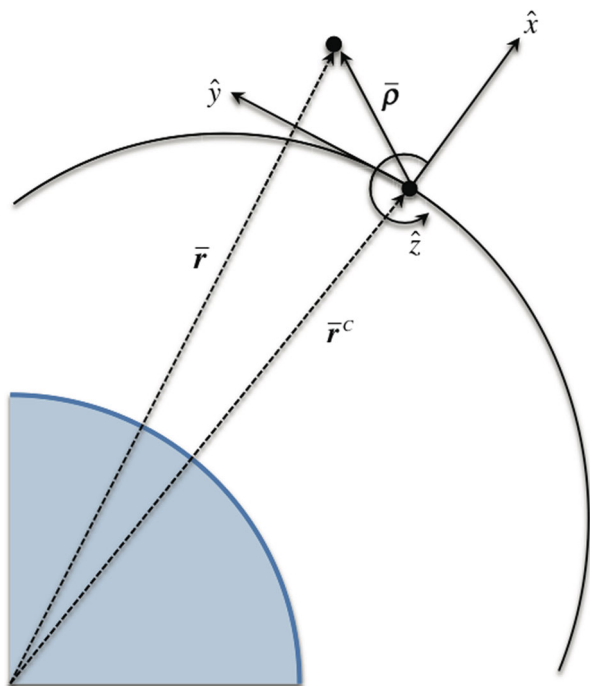
relative true anomaly and relative inclination. It should be noted that other geometric formulations for relative motion exist in the literature (e.g., Ref. [23]), but the formulation presented herein is beneficial in terms of the visualization of the motion and relative orbit design for mission planning.

This article provides a detailed description of the ROE formulation. “**Definition of Relative Orbital Elements**” provides an overview of the derivation of ROEs, and describes the geometric interpretation of each element. The transformation between ROEs and the Cartesian states in the LVLH coordinate frame is developed, and the evolution of ROEs with time is evaluated. “**Characteristics of the Unforced Motion**” describes the three primary modes of the motion, determined based upon the values of the ROEs. Concluding remarks are given in “**Conclusions**”.

Definition of Relative Orbital Elements

In order to describe the ROE formulation, it is assumed that both the chief and deputy spacecraft travel in two-body motion about the central body, with the chief constrained to be on a circular orbit. The central body, chief, and deputy are treated as point masses, and all perturbations are neglected. It is further assumed that the distance from the chief to the deputy is small relative to the chief’s orbit radius. The Clohessy-Wiltshire equations may be expressed in terms of LVLH coordinates. The LVLH frame is defined in Fig. 1. The origin for the LVLH coordinate system is at the chief location. The \hat{x} -axis is in the radial direction, the \hat{z} -axis is in the chief’s angular

Fig. 1 Coordinate system definition for LVLH frame



momentum (cross-track) direction, and the \hat{y} -axis is obtained by $\hat{z} \times \hat{x}$. Note that for a circular chief orbit, the \hat{y} -axis is in the chief’s along-track direction, i.e., aligned with its instantaneous velocity vector. In Fig. 1, the radius vector from the central body to the chief is denoted by $\bar{\mathbf{r}}^C$, the radius to the deputy is denoted by $\bar{\mathbf{r}}$, and the relative position vector from the chief to the deputy is denoted by $\bar{\boldsymbol{\rho}}$.

The Clohessy-Wiltshire equations of motion for the deputy spacecraft relative to the chief are shown in Eqs. 1–3, where n represents the mean motion of the chief spacecraft, and a_{T_x} , a_{T_y} and a_{T_z} are the components of acceleration resulting from external forces acting upon the deputy:

$$\ddot{x} - 2n\dot{y} - 3n^2x = a_{T_x} \tag{1}$$

$$\ddot{y} + 2n\dot{x} = a_{T_y} \tag{2}$$

$$\ddot{z} + n^2z = a_{T_z} \tag{3}$$

For unforced motion, where no thrust is applied to the deputy spacecraft, the Clohessy-Wiltshire equations reduce to Eqs. 4–6:

$$\ddot{x} - 2n\dot{y} - 3n^2x = 0 \tag{4}$$

$$\ddot{y} + 2n\dot{x} = 0 \tag{5}$$

$$\ddot{z} + n^2z = 0 \tag{6}$$

A detailed derivation of the solutions to the Clohessy-Wiltshire equations using Laplace transforms is given in Ref. [19]. If the initial conditions for the LVLH Cartesian state are denoted by the subscript 0, then the position and velocity solutions to the Clohessy-Wiltshire equations are given by Eqs. 7–12:

$$x(t) = \left(4x_0 + \frac{2\dot{y}_0}{n}\right) - \left(3x_0 + \frac{2\dot{y}_0}{n}\right) \cos [n(t - t_0)] + \frac{\dot{x}_0}{n} \sin [n(t - t_0)] \tag{7}$$

$$y(t) = y_0 - \frac{2\dot{x}_0}{n} - (6nx_0 + 3\dot{y}_0)(t - t_0) + \frac{2\dot{x}_0}{n} \cos [n(t - t_0)] + \left(6x_0 + \frac{4\dot{y}_0}{n}\right) \sin [n(t - t_0)] \tag{8}$$

$$z(t) = z_0 \cos [n(t - t_0)] + \frac{\dot{z}_0}{n} \sin [n(t - t_0)] \tag{9}$$

$$\dot{x}(t) = (3nx_0 + 2\dot{y}_0) \sin [n(t - t_0)] + \dot{x}_0 \cos [n(t - t_0)] \tag{10}$$

$$\dot{y}(t) = -(6nx_0 + 3\dot{y}_0) - 2\dot{x}_0 \sin [n(t - t_0)] + (6nx_0 + 4\dot{y}_0) \cos [n(t - t_0)] \tag{11}$$

$$\dot{z}(t) = -nz_0 \sin [n(t - t_0)] + \dot{z}_0 \cos [n(t - t_0)] \tag{12}$$

Derivation of Relative Orbital Elements

Similar to classical orbital elements that convey the orbit geometry of a single space object in orbit about a central body in an inertially-fixed reference frame, ROEs provide a geometric interpretation of the relative orbit between two objects expressed in the LVLH frame. The six ROE parameters fully define the relative orbital state of the deputy with respect to the chief. The ROEs are derived from the solution to

the Clohessy-Wiltshire equations. Application of the Harmonic Addition Theorem to Eqs. 7–9 results in the equations:

$$x(t) = \begin{cases} 4x_0 + \frac{2\dot{y}_0}{n} + \frac{1}{2} \operatorname{sgn} \left[- \left(3x_0 + \frac{2\dot{y}_0}{n} \right) \right] \left[\left(6x_0 + \frac{4\dot{y}_0}{n} \right)^2 + \left(\frac{2\dot{x}_0}{n} \right)^2 \right]^{1/2} \\ \cos \left[n(t - t_0) + \tan^{-1} \left(\frac{\dot{x}_0/n}{3x_0 + \frac{2\dot{y}_0}{n}} \right) \right], 3x_0 + \frac{2\dot{y}_0}{n} \neq 0 \\ 4x_0 + \frac{2\dot{y}_0}{n} + \frac{\dot{x}_0}{n} \sin [n(t - t_0)], 3x_0 + \frac{2\dot{y}_0}{n} = 0 \end{cases} \quad (13)$$

$$y(t) = \begin{cases} y_0 - \frac{2\dot{x}_0}{n} - (6nx_0 + 3\dot{y}_0)(t - t_0) + \operatorname{sgn} \left(\frac{2\dot{x}_0}{n} \right) \\ \cos [n(t - t_0)] + \tan^{-1} \left(-\frac{6\dot{x}_0 + 4\dot{y}_0/n}{2\dot{x}_0/n} \right), \dot{x}_0 \neq 0 \\ y_0 - \frac{2\dot{x}_0}{n} - (6nx_0 + 3\dot{y}_0)(t - t_0) + \left(6\dot{x}_0 + \frac{4\dot{y}_0}{n} \right) \sin [n(t - t_0)], \dot{x}_0 = 0 \end{cases} \quad (14)$$

$$z(t) = \begin{cases} \operatorname{sgn}(z_0) \left[z_0^2 + \left(\frac{\dot{z}_0}{n} \right)^2 \right]^{1/2} \cos \left[n(t - t_0) + \tan^{-1} \left(-\frac{\dot{z}_0/n}{z_0} \right) \right], z_0 \neq 0 \\ \frac{\dot{z}_0}{n} \sin [n(t - t_0)], z_0 = 0 \end{cases} \quad (15)$$

Through introduction of the atan2 function, it can be shown that Eqs. 13–15 may be expressed as:

$$x(t) = 4x_0 + \frac{2\dot{y}_0}{n} - \frac{1}{2} \sqrt{\left(6x_0 + \frac{4\dot{y}_0}{n} \right)^2 + \left(\frac{2\dot{x}_0}{n} \right)^2} \times \cos \left[n(t - t_0) + \operatorname{atan2} \left(\frac{2\dot{x}_0}{n}, 6x_0 + \frac{4\dot{y}_0}{n} \right) \right] \quad (16)$$

$$y(t) = y_0 - \frac{2\dot{x}_0}{n} - (6nx_0 + 3\dot{y}_0)(t - t_0) + \sqrt{\left(6x_0 + \frac{4\dot{y}_0}{n} \right)^2 + \left(\frac{2\dot{x}_0}{n} \right)^2} \sin \left[(t - t_0) + \operatorname{atan2} \left(\frac{2\dot{x}_0}{n}, 6x_0 + \frac{4\dot{y}_0}{n} \right) \right] \quad (17)$$

$$z(t) = \sqrt{z_0^2 + \left(\frac{\dot{z}_0}{n} \right)^2} \sin \left[n(t - t_0) + \operatorname{atan2} \left(z_0, \frac{\dot{z}_0}{n} \right) \right] \quad (18)$$

In Eqs. 16–18, the atan2(*a*, *b*) function is related to the arctangent function $\tan^{-1} \left(\frac{a}{b} \right)$, where $-\pi < \operatorname{atan2}(a, b) \leq \pi$ based upon which quadrant contains the two arguments *a* and *b*. The atan2 function eliminates the need for the sgn function, as well as the need to account for two different cases that appear in each of Eqs. 13–15. Note that for each equation, if both arguments of the atan2(*a*, *b*) function are equal to zero, the coefficient of the sinusoid also equates to zero, resulting in a zero value for the periodic term.

The expressions for the deputy spacecraft position in the orbital plane of the chief spacecraft, (16–17), each have periodic terms and constant terms. The along-track expression (17) also has a term that varies linearly with time, resulting in a secular drift motion. The first two ROEs describe the deputy spacecraft’s instantaneous center of motion relative to the chief, encompassing the constant and linear

time-varying terms. Expressed in terms of the LVLH Cartesian state initial conditions, the instantaneous center of motion ROEs are defined as:

$$x_r = 4x_0 + \frac{2\dot{y}_0}{n} \quad (19)$$

$$y_r = y_0 - \frac{2\dot{x}_0}{n} - (6nx_0 + 3\dot{y}_0)(t - t_0) \quad (20)$$

Equations 19–20 indicate how the instantaneous center of the relative motion moves with time.

From Eq. 17, the amplitude of the sinusoidal motion in the along-track direction is given by:

$$A_y = \sqrt{\left(6x_0 + \frac{4\dot{y}_0}{n}\right)^2 + \left(\frac{2\dot{x}_0}{n}\right)^2} \quad (21)$$

From Eq. 16, the amplitude of the sinusoidal motion in the radial direction is:

$$A_x = \frac{1}{2} \sqrt{\left(6x_0 + \frac{4\dot{y}_0}{n}\right)^2 + \left(\frac{2\dot{y}_0}{n}\right)^2} \quad (22)$$

Note that the amplitude of the sinusoidal motion in the radial direction is half of that in the along-track direction. Thus, the motion in the $\hat{x} - \hat{y}$ plane is always along an “instantaneous ellipse” with the major axis in the along-track direction and with a length that is twice that of the minor axis in the radial direction. Therefore, a single parameter can specify the shape of the instantaneous ellipse in the $\hat{x} - \hat{y}$ plane. This parameter, a_r , is the ROE representing the semimajor axis of the instantaneous relative orbit ellipse, equal to the along-track amplitude of the sinusoidal motion, A_y :

$$a_r = \sqrt{\left(6x_0 + \frac{4\dot{y}_0}{n}\right)^2 + \left(\frac{2\dot{x}_0}{n}\right)^2} \quad (23)$$

The fourth ROE parameterizes the angular position of the chaser spacecraft as it moves along the instantaneous relative orbit ellipse in the $\hat{x} - \hat{y}$ plane. For reasons that are explained below (and shown graphically in Fig. 2) this ROE is termed the relative eccentric anomaly, E_r . It represents the argument of the sine and cosine functions in Eqs. 16 and 17, and can be written:

$$E_r = E_{r_0} + n(t - t_0) \quad (24)$$

where

$$E_{r_0} = \text{atan2}\left(\frac{2\dot{x}_0}{n}, 6x_0 + \frac{4\dot{y}_0}{n}\right) \quad (25)$$

A geometric interpretation of the first four ROE's is shown on an instantaneous relative motion ellipse in Fig. 2. The semimajor axis of the ellipse is given by a_r . The instantaneous center of the ellipse is given by x_r and y_r , and the deputy's periapsis is annotated as point P. The instantaneous deputy position along the ellipse is annotated as point D, with coordinates (x, y) . A circle of radius a_r is circumscribed about the ellipse, and a dashed line, perpendicular to the major axis, is extended through point D, intersecting with the circumscribed circle at point Q. Relative eccentric anomaly,

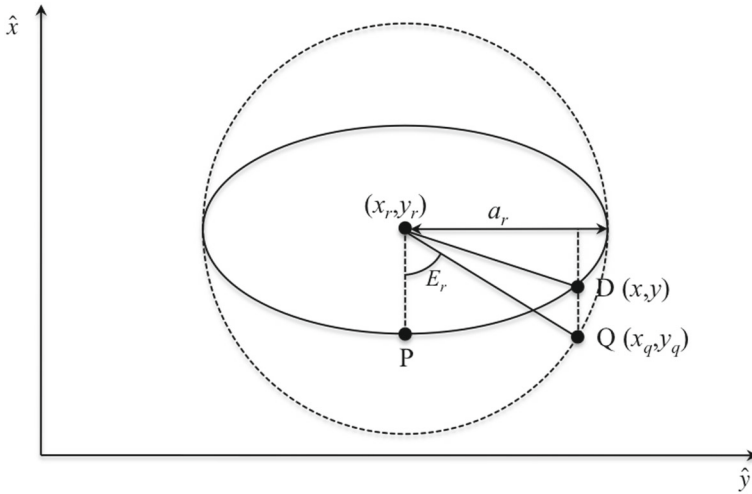


Fig. 2 Relative orbit geometry in the LVLH $\hat{x} - \hat{y}$ plane

E_r , measures the angle centered on (x_r, y_r) , between the periastron point P and point Q. Relative eccentric anomaly increases from zero at periastron with motion in the counter-clockwise direction.

The fifth ROE, A_z , is defined as the amplitude of the sinusoidal motion in the cross-track direction. The cross-track component of the relative motion is a simple harmonic oscillator that is independent of the $\hat{x} - \hat{y}$ motion under the Clohessy-Wiltshire assumptions. From Eq. 18, the amplitude of the cross-track motion is:

$$A_z = \sqrt{z_0^2 + \left(\frac{\dot{z}_0}{n}\right)^2} \tag{26}$$

The sixth ROE, ψ , is defined as the phase angle in the cross-track harmonic motion, representing the argument of the sine function in Eq. 18:

$$\psi = \psi_0 + n(t - t_0) \tag{27}$$

where

$$\psi_0 = \text{atan2}\left(z_0, \frac{\dot{z}_0}{n}\right) \tag{28}$$

A geometric interpretation of A_z and ψ is shown in Fig. 3, where the three-dimensional relative motion is projected onto the $\hat{x} - \hat{z}$ plane. The deputy position along the relative motion ellipse is annotated as initial condition D_0 at time t_0 and as point D at time t . A circle of radius A_z is drawn, with the center of the circle coincident with the center of the ellipse at point C. A dashed line, perpendicular to the \hat{z} -axis, is extended through point D_0 , intersecting with the circumscribed circle at point F_0 . Point G_0 is shown where a line parallel to the \hat{z} -axis through point F_0 intersects the \hat{x} -axis. The angle ψ then represents the angle, centered on point C with coordinates $(x_r, y_r, 0)$, between the $-\hat{x}$ -axis and the segment CF on the circle. The deputy’s relative motion intersects the chief’s orbit plane at $\psi = 0$ and $\psi = \pi$.

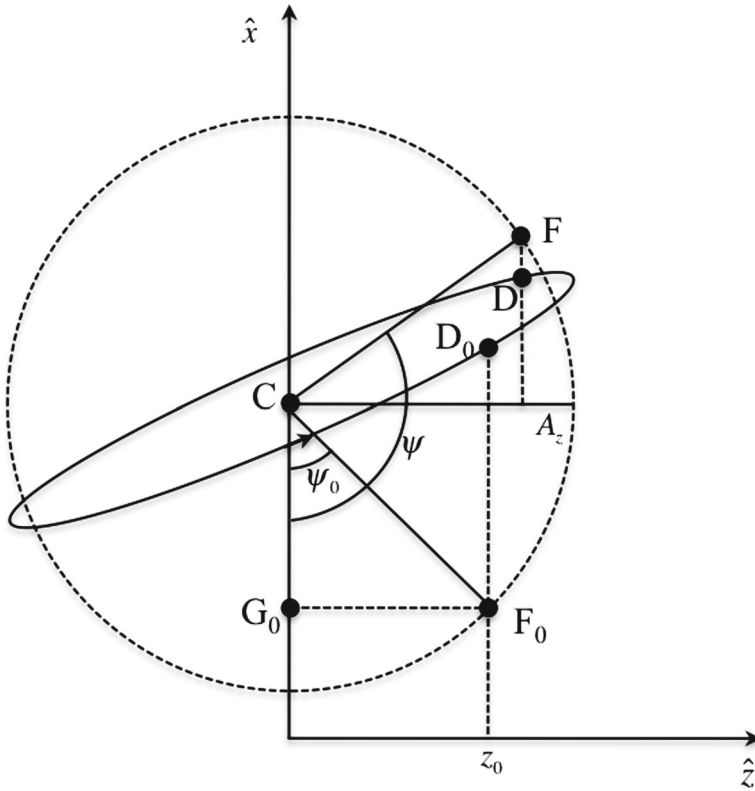


Fig. 3 Cross-track motion phase angle geometry, projected onto the $\hat{x} - \hat{z}$ plane

These points are referred to as the relative ascending and descending nodes, respectively [28, 29]. The relative ascending node is the point where the deputy spacecraft passes through $z = 0$ with $\dot{z} > 0$; the direction of the deputy’s motion is indicated by an arrow in Fig. 3. At $t = t_0$, the cross-track motion phase angle is ψ_0 . As the deputy progresses in its relative motion about the chief, the cross-track motion phase angle changes according to Eq. 27 as point F progresses at a constant rate (equal to the chief’s mean motion) about the circle. At the point in the ellipse where $z = A_z$, $\psi = \frac{\pi}{2}$. The relative descending node occurs at $\psi = \pi$, and $z = -A_z$ at $\psi = -\frac{\pi}{2}$.

Expressions for ROEs in terms of the time-varying Cartesian state elements may be found as follows. Equation 19 may be combined with Eqs. 7 and 11 to show that:

$$x_r = 4x + \frac{2\dot{y}}{n} \tag{29}$$

(For Cartesian state elements without the subscript 0, time dependence is implied.) Likewise, Eq. 20 may be combined with Eqs. 8 and 10 to give:

$$y_r = y - \frac{2\dot{x}}{n} \tag{30}$$

For unforced motion, the time derivative of x_r may be taken using Eq. 29, and by substituting for the \ddot{y} acceleration term using Eq. 5, \dot{x}_r is shown to be equal to zero. Therefore, x_r is invariant with time. However, taking the time derivative of y_r in Eq. 30 and substituting for the \ddot{x} acceleration term using Eq. 4 shows that y_r has a secular drift that varies linearly with time.

Equation 23 may be combined with Eqs. 7, 10, and 11 to show that:

$$a_r = \sqrt{\left(6x + \frac{4\dot{y}}{n}\right)^2 + \left(\frac{2\dot{x}}{n}\right)^2} \tag{31}$$

Taking the time derivative of a_r as expressed in Eq. 31 and substituting for \ddot{x} using Eq. 4 and for \ddot{y} using Eq. 5, it is shown that \dot{a}_r is equal to zero. Therefore, a_r is a constant for unforced motion. Equations 29 – 31 indicate that while the instantaneous center of the motion in the $\hat{x} - \hat{y}$ plane may drift in the along-track direction, its radial component and size are invariant with time.

Equations 24 and 25 may be combined with Eqs. 7, 10, and 11 to show that:

$$E_r = \text{atan2}\left(\frac{2\dot{x}}{n}, 6x + \frac{4\dot{y}}{n}\right) \tag{32}$$

From Eq. 24, it is seen that the time derivative of E_r is equal to n .

Equation 26 may be combined with Eqs. 9 and 12 to show that:

$$A_z = \sqrt{z^2 + \left(\frac{\dot{z}}{n}\right)^2} \tag{33}$$

Taking the time derivative of A_z as expressed in Eq. 33, and substituting for the \dot{z} term using Eq. 6, it is shown that \dot{A}_z is equal to zero. Therefore, A_z is a constant of the unforced motion.

Equations 27 and 28 may be combined with Eqs. 9 and 12 to show that:

$$\psi = \text{atan2}\left(z, \frac{\dot{z}}{n}\right) \tag{34}$$

From Eq. 27, it is seen that the time derivative of ψ is equal to n .

Table 1 summarizes the expressions for the six ROEs in terms of the LVLH Cartesian states, both at the initial time and at any instantaneous time.

Transformation from Relative Orbital Elements to LVLH Cartesian State

It is frequently desirable to be able to transform from ROEs to LVLH Cartesian states. These transformations are developed here. The position components of the LVLH Cartesian state can be found as follows: Eqs. 19, and 23–25 may be substituted into Eq. 16 to yield:

$$x = x_r - \frac{1}{2}a_r \cos E_r \tag{35}$$

Similarly, Eqs. 20 and 23–25 may be substituted into Eq. 17 to give:

$$y = y_r + a_r \sin E_r \tag{36}$$

Table 1 Expressions for ROEs in terms of LVLH Cartesian state elements

Relative Orbital Element	Expressed in terms of LVLH Cartesian State Initial Conditions	Expressed in terms of Instantaneous LVLH Cartesian State Elements
x_r	$4x_0 + \frac{2\dot{y}_0}{n}$	$4x + \frac{2\dot{y}}{n}$
y_r	$y_0 - \frac{2\dot{x}_0}{n} - (6nx_0 + 3\dot{y}_0)(t - t_0)$	$y - \frac{2\dot{x}}{n}$
a_r	$\sqrt{\left(6x_0 + \frac{4\dot{y}_0}{n}\right)^2 + \left(\frac{2\dot{x}_0}{n}\right)^2}$	$\sqrt{\left(6x + \frac{4\dot{y}}{n}\right)^2 + \left(\frac{2\dot{x}}{n}\right)^2}$
E_r	$\text{atan2}\left(\frac{2\dot{x}_0}{n}, 6x_0 + \frac{4\dot{y}_0}{n}\right) + n(t - t_0)$	$\text{atan2}\left(\frac{2\dot{x}}{n}, 6x + \frac{4\dot{y}}{n}\right)$
A_z	$\sqrt{z_0^2 + \left(\frac{\dot{z}_0}{n}\right)^2}$	$\sqrt{z^2 + \left(\frac{\dot{z}}{n}\right)^2}$
ψ	$\text{atan2}\left(z_0, \frac{\dot{z}_0}{n}\right) + n(t - t_0)$	$\text{atan2}\left(z, \frac{\dot{z}}{n}\right)$

Equations 26–28 may be substituted into Eq. 18 to give:

$$z = A_z \sin \psi \tag{37}$$

The velocity LVLH state components can be found as follows. Equation 30 may be substituted into Eq. 36 and rearranged to yield:

$$\dot{x} = \frac{n}{2} a_r \sin E_r \tag{38}$$

Equation 29 can be substituted into Eq. 35 and rearranged to give:

$$\dot{y} = -\frac{3}{2} nx + na_r \cos E_r \tag{39}$$

Equation 29 can be rewritten as:

$$x = \frac{x_r}{4} - \frac{\dot{y}}{2n} \tag{40}$$

Substituting Eq. 40 into 39 and solving for \dot{y} gives:

$$\dot{y} = -\frac{3}{2} nx_r + na_r \cos E_r \tag{41}$$

Rearranging Eq. 33 gives:

$$\dot{z}^2 = n^2 \left(A_z^2 - z^2 \right) \tag{42}$$

Substituting Eq. 37 into 42 gives:

$$\dot{z} = n^2 A_z^2 \cos^2 \psi \tag{43}$$

Taking the square root of both sides of Eq. 43 gives:

$$\dot{z} = \pm n A_z \cos \psi \tag{44}$$

Referencing Fig. 3, because $\dot{z} > 0$ when $\psi = 0$, then

$$\dot{z} = n A_z \cos \psi \tag{45}$$

A summary of the transformation from ROEs to LVLH Cartesian state elements is given in Table 2.

Table 2 Expressions for LVLH Cartesian state elements in terms of ROEs

LVLH Cartesian State Element	Expressed in Terms of ROEs
x	$x_r - \frac{1}{2}a_r \cos E_r$
y	$y_r + a_r \sin E_r$
z	$A_z \sin \psi$
\dot{x}	$\frac{n}{2}a_r \sin E_r$
\dot{y}	$-\frac{3}{2}nx_r + na_r \cos E_r$
\dot{z}	$nA_z \cos \psi$

Evolution of Relative Orbital Elements with Time

Previously, expressions for the time variation of ROEs were developed in terms of LVLH Cartesian state elements. In this section, expressions for the time variation of each ROE are developed in terms of initial ROE values. The initial condition for each ROE at time t_0 is denoted with a subscript 0.

Equations 19 and 20 express the variation of the instantaneous center of motion with time, given initial conditions expressed in terms of the LVLH Cartesian state. From Eq. 19, it is clear that at $t = t_0$:

$$x_{r0} = 4x_0 + \frac{2\dot{y}_0}{n} \tag{46}$$

As described in “Derivation of Relative Orbital Elements”, the radial coordinate of the instantaneous center of the motion is shown to be constant for unforced motion:

$$x_r = x_{r0} \tag{47}$$

Evaluating (20) at $t = t_0$ yields:

$$y_{r0} = y_0 - \frac{2\dot{x}_0}{n} \tag{48}$$

Multiplying (19) by a factor of $\frac{3n}{2}$, and substituting with Eq. 48 into Eq. 20 gives:

$$y_r = y_{r0} - \left(\frac{3}{2}\right)nx_{r0}(t - t_0) \tag{49}$$

As discussed in “Derivation of Relative Orbital Elements”, for unforced motion a_r does not vary as a function of time:

$$a_r = a_{r0} \tag{50}$$

Relative eccentric anomaly varies with time as expressed in Eq. 24, and repeated here:

$$E_r = E_{r0} + n(t - t_0) \tag{51}$$

The amplitude of the cross-track motion, A_z , is given by Eq. 26 as a function of the LVLH Cartesian state initial conditions. Once established by the initial conditions, A_z does not vary with time, therefore:

$$A_z = A_{z0} \tag{52}$$

Finally, the phase angle in the cross-track harmonic motion is given by Eq. 27, repeated here:

$$\psi = \psi_0 + n(t - t_0) \quad (53)$$

In summary, for unforced motion the ROEs x_r , a_r and A_z remain constant, y_r varies linearly with time proportional to the secular drift rate, while the angular ROEs E_r and ψ vary at a constant angular rate equal to the chief's mean motion, n . A summary of the expressions for ROEs in terms of the ROE initial conditions is provided in Table 3.

Additional Parameters Related to Relative Orbital Elements

In addition to the ROEs summarized in Table 1, there are several related parameters that provide insight into the relative motion. The additional parameters described here include along-track secular drift and drift rate, relative true anomaly, phase angle difference, and relative inclination.

Along-Track Secular Drift and Drift rate

The linear time-varying along-track secular drift term in Eq. 17 indicates the direction and rate of the instantaneous center of motion in the $\hat{x} - \hat{y}$ plane. The secular drift parameter y_s is defined as:

$$y_s = -(6nx_0 + 3\dot{y}_0)(t - t_0) \quad (54)$$

In Eq. 54, y_s equals the distance in the along-track direction that the instantaneous center of motion has moved during the time period $t - t_0$. At a given time, the secular drift rate can be written as:

$$\dot{y}_s = (6nx_0 + 3\dot{y}_0) \quad (55)$$

For unforced motion, the secular drift rate is a constant. By taking the time derivative of Eq. 20, it is clear that \dot{y}_s is equivalent to \dot{y}_r . From Eqs. 19 and 55, it is apparent that:

$$\dot{y}_s = \frac{3}{2}nx_r \quad (56)$$

Thus, the secular drift rate of the instantaneous ellipse in the $\hat{x} - \hat{y}$ plane is negatively proportional to the radial coordinate of the instantaneous center of motion; if x_r is

Table 3 Expressions for ROEs in terms of ROE initial conditions

Relative Orbital Element	Expressed in terms of ROE Initial Conditions
x_r	x_{r0}
y_r	$y_{r0} - \frac{3}{2}nx_{r0}(t - t_0)$
a_r	a_{r0}
E_r	$E_{r0} + n(t - t_0)$
A_z	A_{z0}
ψ	$\psi_0 + n(t - t_0)$

greater than zero, the secular drift is in the negative along-track direction, and vice-versa. If x_r equals zero, there is no drift. From Eqs. 20 and 55 it can be seen that:

$$y_r = y_{r0} + \dot{y}_s (t - t_0) \tag{57}$$

where

$$y_{r0} = y_0 - \frac{2\dot{x}_0}{n} \tag{58}$$

An example is shown in Fig. 4. The initial coordinates of the instantaneous center of motion in the $\hat{x} - \hat{y}$ plane at $t - t_0$ are (x_{r0}, y_{r0}) . Three orbit periods later, the instantaneous center coordinates are (x_r, y_r) . In this case, $x_{r0} > 0$, so \dot{y}_s is negative, and the secular drift is from right to left, in the negative along-track direction. Secular drift rate may be used as an alternative to x_r within the set of ROEs.

Relative true Anomaly

An angle termed relative true anomaly may be defined that is analogous to the classical orbital element true anomaly, except that it is defined strictly in the $\hat{x} - \hat{y}$ plane. As shown in Fig. 5, relative true anomaly, ν_r , is the angle, centered on (x_r, y_r) , between the periapsis point P and point D, the instantaneous deputy position along the ellipse. Point Q on the circumscribed circle is always twice as far as point D from the semi-major axis of the instantaneous relative motion ellipse. This can be shown as follows.

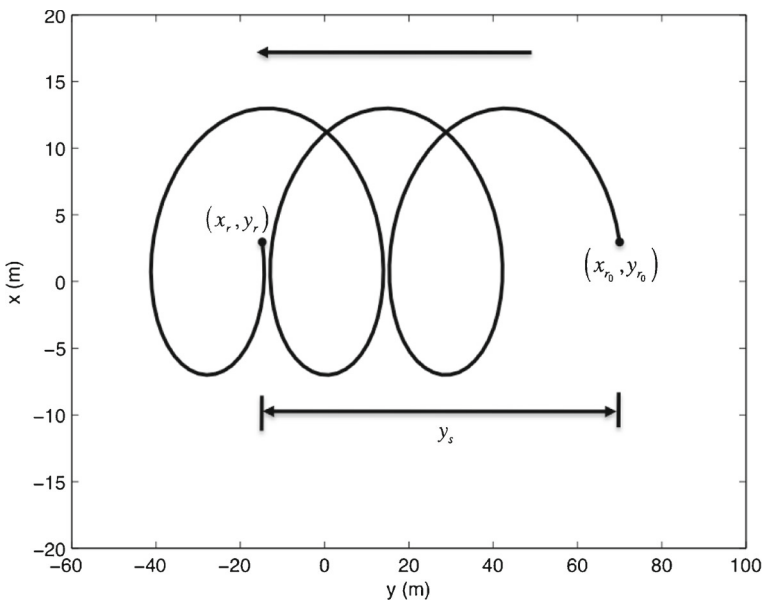


Fig. 4 Secular along-track drift in the $\hat{x} - \hat{y}$ plane

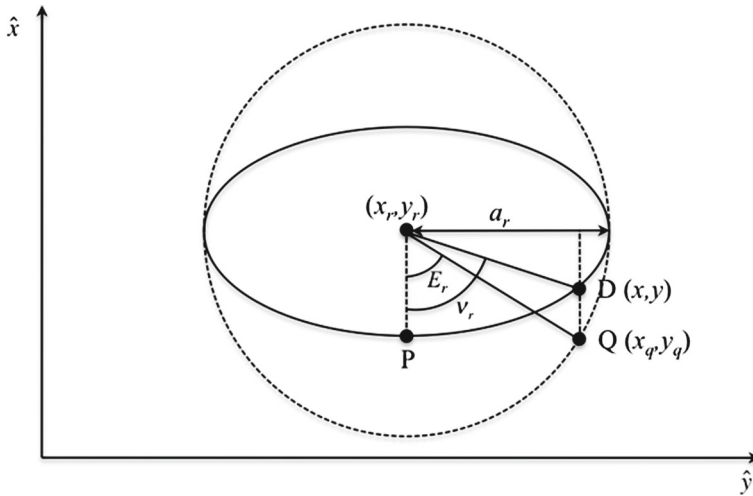


Fig. 5 Geometry of relative eccentric anomaly and relative true anomaly

From the standard equation of an ellipse, the instantaneous relative motion ellipse equation is:

$$\frac{(y - y_r)^2}{a_r^2} + \frac{(x - x_r)^2}{\left(\frac{a_r}{2}\right)^2} = 1 \tag{59}$$

Solving (38) for $x - x_r$ gives:

$$x - x_r = \frac{1}{2} \sqrt{a_r^2 - (y - y_r)^2} \tag{60}$$

From the standard equation for a circle, the equation for the circumscribed circle can be written as:

$$\frac{(y_q - y_r)^2}{a_r^2} + \frac{(x_q - x_r)^2}{a_r^2} = 1 \tag{61}$$

Solving (61) for $x_q - x_r$, and noting that $y_q = y$, gives:

$$x_q - x_r = \sqrt{a_r^2 - (y - y_r)^2} \tag{62}$$

From Eqs. 60 and 62, the desired result is obtained:

$$x - x_r = \frac{1}{2} (x_q - x_r) \tag{63}$$

From Fig. 5 it is clear that:

$$\tan E_r = \frac{y - y_r}{2(x_r - x)} \tag{64}$$

Substituting for x_r and y_r in Eq. 64 using Eqs. 29 and 30 and simplifying gives:

$$\tan E_r = \frac{\dot{x}}{3nx + 2\dot{y}} \tag{65}$$

From Fig. 5, it is apparent that:

$$\tan \nu_r = \frac{y - y_r}{x_r - x} \tag{66}$$

Substituting for x_r and y_r in Eq. 66 using Eqs. 29 and 30 and simplifying, yields:

$$\tan \nu_r = \frac{2\dot{x}}{3nx + 2\dot{y}} \tag{67}$$

Therefore, relative true anomaly can be expressed as:

$$\nu_r = \tan^{-1} \left(\frac{2\dot{x}}{3nx + 2\dot{y}} \right) \tag{68}$$

Comparing Eq. 68 with Eq. 65, the relationship between relative eccentric anomaly and relative true anomaly is then:

$$\nu_r = \tan^{-1} (2 \tan E_r) \tag{69}$$

Relative true anomaly may be used as an alternative to relative eccentric anomaly within the set of ROEs.

Phase Angle Difference

The phase angle difference between the relative eccentric anomaly, E_r , and the cross-track motion phase angle, ψ , can be expressed as:

$$\gamma = \psi - E_r \tag{70}$$

The cross-track motion phase angle and relative eccentric anomaly both change at a rate that is equal to the chief’s mean motion, as seen in Eqs. 24 and 27. Therefore, the phase difference γ is a constant, equal to the difference between the two angles at any chosen instant in time. Equation 70 may be used to replace ψ with $\gamma + E_r$. The advantage of this approach is that four of the six ROEs are then constant, with y_r and E_r being the only time-varying ROEs. (Note that one could alternatively replace E_r with $\psi - \gamma$ and also achieve four constant ROEs.) The phase difference may be written in terms of LVLH Cartesian state elements as:

$$\gamma = \text{atan2} \left(z, \frac{\dot{z}}{n} \right) - \text{atan2} \left(\frac{2\dot{x}}{n}, 6x + \frac{4\dot{y}}{n} \right) \tag{71}$$

Relative Inclination

An important parameter related to the three-dimensional relative motion is the relative inclination, the angle between the relative orbit plane and the chief’s orbit plane (i.e., the $\hat{x} - \hat{y}$ plane). As shown in Fig. 6, the normal vector to the instantaneous relative orbit plane, \hat{n}_r , is found by taking the cross-product of two position vectors on the relative orbit, corresponding to $E_r = 0$ and $E_r = \frac{\pi}{2}$. In Fig. 6, the LVLH $\hat{z} - \hat{y} - \hat{z}$ coordinate system is translated to parallel axes $\hat{z}' - \hat{y}' - \hat{z}'$ with the origin at $(x_r, y_r, 0)$. The relative inclination is the angle between the relative orbit normal, \hat{n}_r and the \hat{z}' axis.

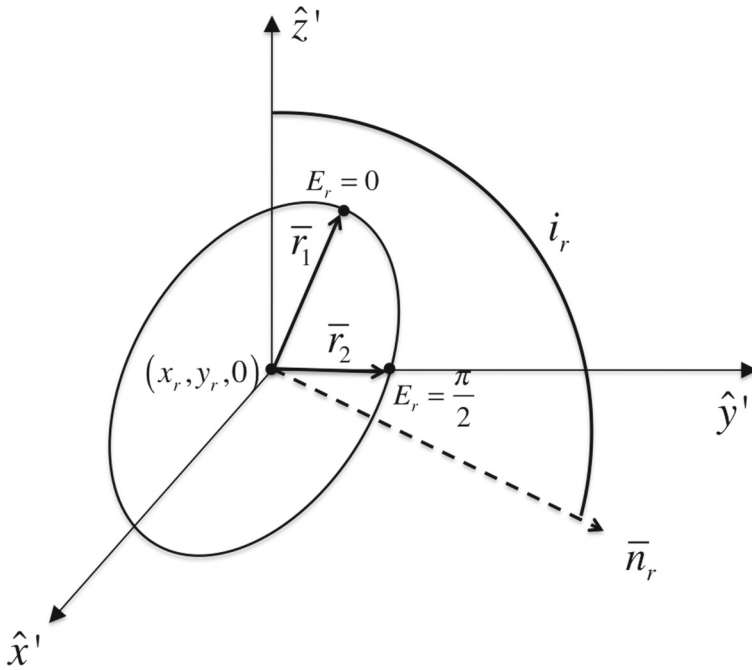


Fig. 6 Geometry of relative inclination

The position of the instantaneous center (IC) of the relative motion with respect to the origin of the LVLH coordinate system is given by the vector:

$$\bar{\rho}^{IC} = [x_r, y_r, 0]^T \tag{72}$$

The vector from the origin of the LVLH coordinate system to the relative orbit position corresponding to $E_r = 0$ (periapsis) is given by Eqs. 35 – 37 as:

$$\bar{\rho}_1 = \begin{bmatrix} x_r - \frac{1}{2}a_r \\ y_r \\ A_z \sin \gamma \end{bmatrix} \tag{73}$$

where, from Eq. 70, γ is equal to ψ for $E_r = 0$. The position vector from the instantaneous center to the location on the relative orbit corresponding to $E_r = 0$ is given by:

$$\bar{r}_1 = \bar{\rho}_1 - \bar{\rho}^{IC} \tag{74}$$

From Eqs. 72 – 74, \bar{r}_1 can be evaluated as:

$$\bar{r}_1 = \begin{bmatrix} -\frac{1}{2}a_r \\ 0 \\ A_z \sin \gamma \end{bmatrix} \tag{75}$$

The vector from the origin of the LVLH coordinate system to the relative orbit position corresponding to $E_r = \frac{\pi}{2}$ is:

$$\bar{\rho}_2 = \begin{bmatrix} x_r \\ y_r + a_r \\ A_z \cos \gamma \end{bmatrix} \tag{76}$$

Note that for $E_r = \frac{\pi}{2}, \gamma = \psi - \frac{\pi}{2}$. From Eq. 37, the \hat{z} -component of the position vector is equal to $A_z \sin \psi$, which equates to $A_z \sin(\gamma + \frac{\pi}{2})$ for $E_r = \frac{\pi}{2}$. This is simplified to $A_z \cos \gamma$ in Eq. 76. The position vector from the instantaneous center to the deputy at $E_r = \frac{\pi}{2}$ is given by:

$$\bar{\mathbf{r}}_2 = \bar{\rho}_2 - \bar{\rho}^{IC} \tag{77}$$

From Eqs 72, 76 and 77, $\bar{\mathbf{r}}_2$ can be evaluated as:

$$\bar{\mathbf{r}}_2 = \begin{bmatrix} 0 \\ a_r \\ A_z \cos \gamma \end{bmatrix} \tag{78}$$

Using the two position vectors on the instantaneous relative orbit, the cross-product can be taken to find the relative orbit normal, $\bar{\mathbf{n}}_r$:

$$\bar{\mathbf{n}}_r = \bar{\mathbf{r}}_1 \times \bar{\mathbf{r}}_2 \tag{79}$$

Using Eqs. 75 and 78, the relative orbit normal vector can be evaluated as:

$$\bar{\mathbf{n}}_r = \begin{bmatrix} -a_r A_z \sin \gamma \\ \frac{1}{2} a_r A_z \cos \gamma \\ -\frac{1}{2} a_r^2 \end{bmatrix} \tag{80}$$

The unit vector in the direction of the relative orbit normal is given by:

$$\hat{\mathbf{n}}_r = \frac{\bar{\mathbf{n}}_r}{|\bar{\mathbf{n}}_r|} \tag{81}$$

The relative inclination, i_r , is the angle between the instantaneous relative orbit plane and the chief orbit plane. The angle between the relative orbit normal and the chief’s orbit normal, $\hat{\mathbf{z}}$, can be found through the dot product of the two normal unit vectors:

$$\hat{\mathbf{n}}_r \cdot \hat{\mathbf{z}} = \cos i_r \tag{82}$$

The relative inclination is given by:

$$i_r = \cos^{-1} (\hat{\mathbf{n}}_r \cdot \hat{\mathbf{z}}) \tag{83}$$

Substituting Eqs. 80 and 81 into 83 and simplifying yields:

$$i_r = \cos^{-1} \left(\frac{-a_r}{\sqrt{3A_z^2 \sin^2 \gamma + A_z^2 \cos^2 \gamma + a_r^2}} \right) \tag{84}$$

From Eq. 84, it is seen that relative inclination is a function of the semi-major axis of the instantaneous relative ellipse in the $\hat{x} - \hat{y}$ plane, a_r , the amplitude of the cross-track motion, A_z , and the phase difference, γ . For unforced motion, each

of these parameters is constant, so relative inclination is a constant as well. If the relative ellipse has a secular along-track drift rate due to a non-zero value for x_r , the instantaneous relative ellipse lies in a plane that is translating in the along-track direction, with a constant relative inclination angle. Note that for relative motion constrained to the direction, resulting in a relative inclination of 180 deg. Because i_r is a function of a_r , A_z , and γ , it may be used to replace any of these three quantities within the set of ROEs.

To express relative inclination in terms of LVLH Cartesian state elements, Eqs. 31, 33 and 71 are substituted into Eq. 84 to give:

$$i_r = \cos^{-1} \left\{ \frac{-\sqrt{\left(6x + \frac{4\dot{y}}{n}\right)^2 + \left(\frac{2\dot{x}}{n}\right)^2}}{\sqrt{3 \left[z^2 + \left(\frac{\dot{z}}{n}\right)^2 \right] \sin^2 \left[\text{atan2} \left(z, \frac{\dot{z}}{n} \right) - \text{atan2} \left(\frac{2\dot{x}}{n}, 6x + \frac{4\dot{y}}{n} \right) \right] + z^2 + \left(\frac{\dot{z}}{n}\right)^2 + \left(6x + \frac{4\dot{y}}{n}\right)^2 + \left(\frac{2\dot{x}}{n}\right)^2}} \right\} \tag{85}$$

A summary of the useful parameters that are related to ROEs is provided in Table 4.

Characteristics of the Unforced Motion

Utilizing the ROEs defined in “Definition of Relative Orbital Elements”, the unforced “free drift” deputy spacecraft trajectory relative to the chief can be easily characterized. Similar to classical orbital elements, ROEs provide a physical understanding of the relative motion that is not obvious from the relative Cartesian state.

The relative motion is characterized in terms of three primary modes of the motion, based upon the values of the ROEs x_d , a_r , and A_z . As seen in Table 5, the first mode of the relative motion is dependent upon the value for x_r . If $x_r = 0$ (Mode 1A), then there is no secular drift of the relative motion in the along-track direction. If $x_r \neq 0$ (Mode 1B), then the instantaneous relative ellipse in the $\hat{x} - \hat{y}$ plane will have a secular drift with a rate that is dependent upon the value for x_r : a negative value for x_r results in a positive secular drift rate in the along-track direction, and a positive value for x_r results in a negative rate for secular along-track drift. Note that this behavior makes physical sense when one considers that $x_r = 0$ implies that the chief and deputy possess the same orbit period, $x_r > 0$ implies that the deputy is on a

Table 4 Expressions for useful parameters related to ROEs

Parameter	Expressed in terms of LVLH Cartesian State Elements	Expressed in terms of ROEs
y_s	$-(6nx_0 + 3\dot{y}_0)(t - t_0)$	$-\frac{3}{2}nx_{r0}(t - t_0)$
\dot{y}_s	$-(6n\dot{x} + 3\ddot{y})$	$-\frac{3}{2}n\dot{x}_r$
v_r	$\tan^{-1} \left(\frac{2\dot{x}}{3n\dot{x} + 2\ddot{y}} \right)$	$\tan^{-1} (2 \tan E_r)$
γ	$\text{atan2} \left(z, \frac{\dot{z}}{n} \right) - \text{atan2} \left(\frac{2\dot{x}}{n}, 6x + \frac{4\dot{y}}{n} \right)$	$\psi - E_r$
i_r	See Eq. 85	$\cos^{-1} \left(\frac{-a_r}{\sqrt{3A_z^2 \sin^2 \gamma + A_z^2 \cos^2 \gamma + a_r^2}} \right)$

Table 5 Modes of unforced relative motion

Mode	Initial Condition	Description
1	1A $x_r = 0$	No secular along-track drift of instantaneous ellipse
	1B $x_r \neq 0$	Secular along-track drift of instantaneous ellipse : $x_r > 0 \Rightarrow \dot{y}_s < 0$ $x_r < 0 \Rightarrow \dot{y}_s > 0$
2	2A $a_r = 0$	No instantaneous ellipse in the $\hat{x} - \hat{y}$ plane
	2B $a_r > 0$	Instantaneous ellipse in the $\hat{x} - \hat{y}$ plane
3	3A $A_z = 0$	No cross-track motion
	3B $A_z > 0$	Simple harmonic oscillatory cross-track motion

larger inertial orbit (longer period) than the chief, and $x_r < 0$ implies that the deputy is on a smaller orbit (shorter period) than the chief.

The second mode of the relative motion depends upon the value for a_r . If $a_r = 0$ (Mode 2A), then there is no instantaneous relative ellipse in the $\hat{x} - \hat{y}$ plane. Stated differently, the instantaneous relative ellipse devolves to a point. If $a_r > 0$ (Mode 2B), then the instantaneous relative ellipse in the $\hat{x} - \hat{y}$ plane has the typical 2:1 ratio of semi-major axis in the along-track direction to semiminor axis in the radial direction. This behavior makes physical sense when one considers that $a_r = 0$ implies that the chief and deputy are both on circular orbits, whereas $a_r > 0$ implies that the deputy is on an elliptical inertial orbit.

The third mode of the relative motion is dependent upon the value for A_z . If $A_z = 0$ (Mode 3A), then there is no cross-track motion. If $A_z > 0$ (Mode 3B), then there is simple harmonic oscillatory motion in the cross-track direction. It is noted that the initial value for y_r does not define a primary mode for the relative motion; y_r simply gives the initial along-track coordinate of the instantaneous relative ellipse in the $\hat{x} - \hat{y}$ plane. The angular ROEs E_r and ψ are used to define the location of the deputy on the relative orbit in-plane and out-of-plane of the chief’s orbit, respectively. The phasing between these angles impacts the three-dimensional shape of the relative orbit, and determines the locations of the relative ascending and descending nodes where the deputy’s inertial trajectory intersects the chief’s orbit plane.

Each of the three primary modes of relative motion can be superposed to capture the full motion of the deputy spacecraft relative to the chief. For Mode 1A, there is no secular drift in the along-track direction, so the motion in the $\hat{x} - \hat{y}$ plane is either a stationary point with $x = 0$ (Mode 1A, 2A), or a stationary ellipse (Mode 1A, 2B) with the characteristic 2:1 ratio of the major-axis to minor-axis length in the $\hat{x} - \hat{y}$ plane.

For Mode 1B, where there is a secular drift of the instantaneous ellipse in the along-track direction, the $\hat{x} - \hat{y}$ projection of the deputy’s motion will take on one of four different shapes. Figure 7 shows an example of each of these relative motion shapes, for a case where the chief’s circular orbit altitude is 500 km, the initial along-track coordinate for the deputy is 100 m, and x_r for the deputy is 5 m, resulting in a negative secular drift rate in the along-track direction. One orbit period is shown.

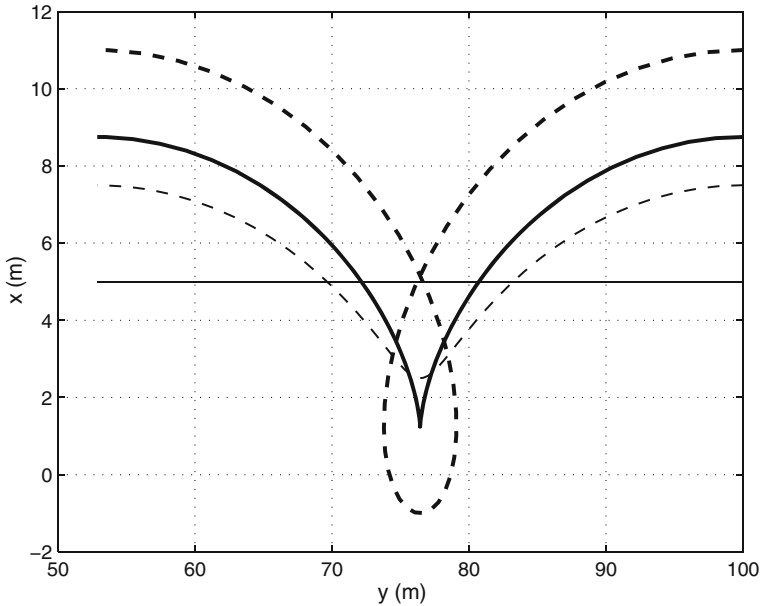


Fig. 7 Four types of relative drifting motion in the $\hat{x} - \hat{y}$ plane. Mode 1B, 2A: solid line, $a_r = 0$. Mode 1B, 2B: dashed quasi-sinusoidal curve, $a_r < \frac{3}{2}|x_r|$; bolded cycloid-like curve with cusp, $a_r = \frac{3}{2}|x_r|$; bold-dashed cycloid-like curve with curl, $a_r > \frac{3}{2}|x_r|$. In all cases, motion is from right to left

The shape of the relative drifting motion in the $\hat{x} - \hat{y}$ plane is determined by the value of a_r relative to x_r . For $a_r = 0$ (Mode 1B, 2A), the deputy is on a circular orbit, and the motion with respect to the chief is a straight line in the LVLH frame, with a fixed radial component. For $a_r > 0$ (Mode 1B, 2B), the relative motion may be a quasi-sinusoidal curve, a cycloid-like curve that cusps at the extrema, or a cycloid-like curve that curls at the extrema. For all three of the cases in Mode 1B, 2B, the minimum radial coordinate occurs at perigee in the deputy’s orbit, and the maximum radial coordinate occurs at apogee. The quasi-sinusoidal curve is produced when the along-track component of the LVLH Cartesian state increases or decreases monotonically.

Substituting Eq. 35 into Eq. 39, and using Eq. 56 it is found that:

$$\dot{y} = \dot{y}_s + na_r \cos E_r \tag{86}$$

For the case where the along-track component is monotonically decreasing (as shown by the dashed curve in Fig. 7),

$$\dot{y}_s + na_r < 0 \tag{87}$$

Substituting for \dot{y}_s with Eq. 56 gives:

$$a_r < \frac{3}{2}x_r \tag{88}$$

Written generally, to account for both the monotonically increasing and decreasing cases, the condition for a quasi-sinusoidal curve can be written as:

$$a_r \frac{3}{2} |x_r| \tag{89}$$

For a cycloid-like curve that cusps, $\dot{y} = 0$ at either periapsis or apoapsis in the deputy’s orbit (i.e., at E_r or $E_r = \pi$). From Eq. 86, it is found that the condition reduces to:

$$a_r = \frac{3}{2} |x_r| \tag{90}$$

It is noted that for the case where the secular drift rate in the along-track direction is negative, cusps occur at perigee (as shown by the bolded curve in Fig. 8), while for a positive secular drift rate cusps occur at apogee. Finally, cycloid-like curves that curl occur for all other values of a_r , when:

$$a_r = \frac{3}{2} |x_r| \tag{91}$$

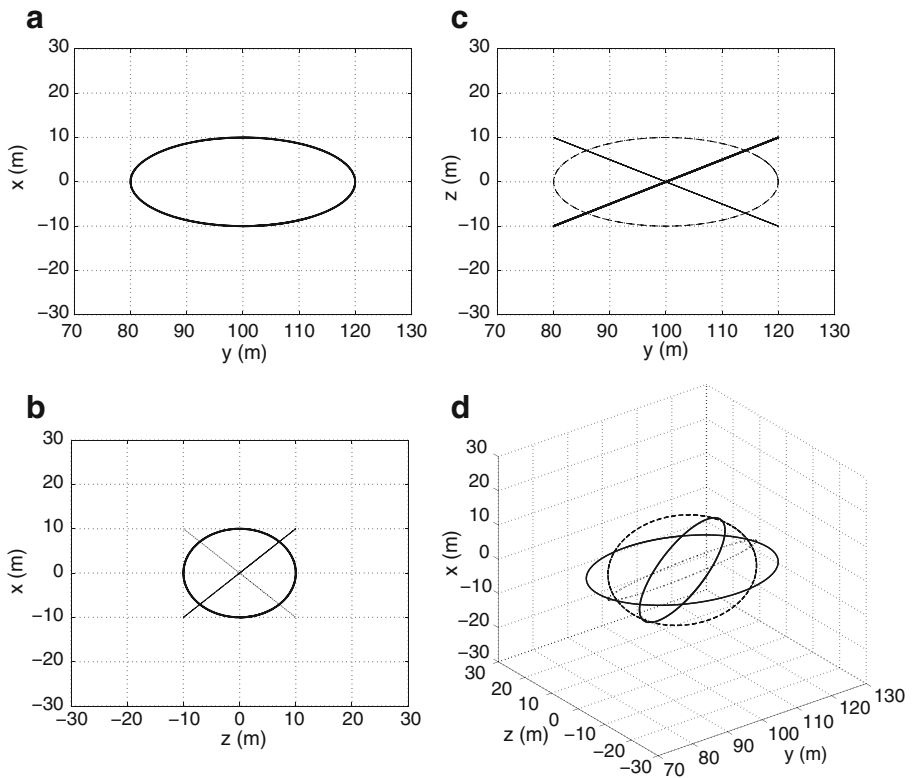


Fig. 8 Mode 1A, 2B, 3B motion with varying phase difference, γ . Bold solid line: $\gamma = 0$; dashed line: $\gamma = \pi/2$; solid line: $\gamma = \pi$; dotted line: $\gamma = 3\pi/2$. **a** $\hat{y} - \hat{x}$ projection, **b** $\hat{z} - \hat{x}$ projection, **c** $\hat{y} - \hat{z}$ projection, **d** 3D plot

For Mode 3A, there is no cross-track motion and $z = 0$. For the combination of Modes 1A, 2A, 3B, the motion is a simple oscillation in the cross-track direction, and there is no motion in the $\hat{x} - \hat{y}$ plane.

For Mode 1A, 2B, 3B, the relative orbit is stationary and in a fixed plane. The angular difference between the relative eccentric anomaly and cross-track phase angle (equal to the parameter γ defined in “Derivation of Relative Orbital Elements”) determines the shape and orientation of the projection of the motion in the $\hat{z} - \hat{x}$ and $\hat{z} - \hat{y}$ planes, as shown in Fig. 8. The motion in the $\hat{x} - \hat{z}$ plane is an ellipse centered on $x = 0, z = 0$. The motion in the $\hat{y} - \hat{z}$ plane is an ellipse centered on $y = y_r, z = 0$. Figure 8 shows an example where $x_r = 0, y_r = 100$ m, $a_r = 20$ m, and $A_z = 10$ m. Relative orbits associated with four different values for γ are shown: $0, \pi/2, \pi,$ and $3\pi/2$. While the motion in the $\hat{x} - \hat{y}$ plane is unchanged for each case, the shape and orientation of the ellipses in the $\hat{x} - \hat{z}$ and $\hat{y} - \hat{z}$ planes are determined by the value of γ . Note that for $\gamma = \pi/2$ and $\gamma = 3\pi/2$, the projection of the motion onto the $\hat{x} - \hat{z}$ and $\hat{y} - \hat{z}$ planes are straight lines.

For Mode 1B, 2B, 3B, a secular along-track drift is superimposed upon the three-dimensional relative motion. Figure 9 shows an example where $x_r = 1$ m, $y_r = 100$ m, $a_r = 20$ m, $A_z = 10$ m, and $\gamma = 0$. The “corkscrew” motion apparent in the three-dimensional plot, Fig. 9d, results from the translation of the instantaneous plane of the motion in the along-track direction.

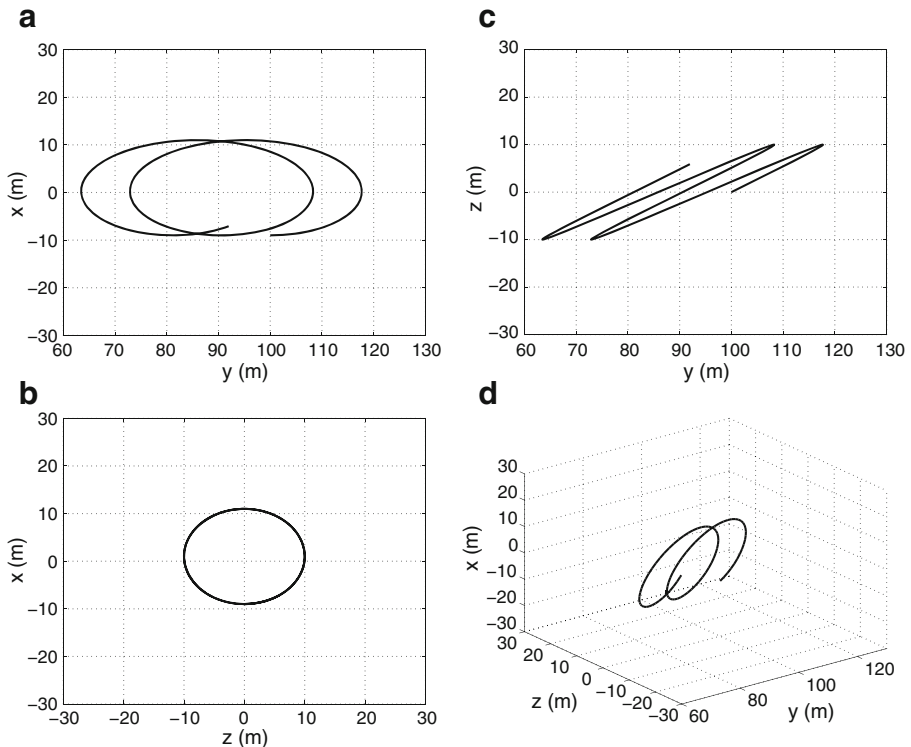


Fig. 9 Mode 1B, 2B, 3B motion. **a** $\hat{y} - \hat{x}$ projection, **b** $\hat{z} - \hat{x}$ projection, **c** $\hat{z} - \hat{y}$ projection, **d** 3D plot

Conclusions

Relative orbital elements provide a useful formulation for characterizing the geometry of relative motion between a chief and deputy space object, leading to an intuitive understanding of the unforced relative motion within the context of the Clohessy-Wiltshire assumptions. Through this work, ROEs have been derived, and the geometric interpretation of each element has been established. It is noted that there is a strong analogy between classical orbital elements, which provide the orbital geometry of a spacecraft about a central body in an inertial reference frame under the two-body assumption, and ROEs which provide the geometry of a relative orbit in the LVLH reference frame under the Clohessy-Wiltshire assumptions.

A direct transformation between ROEs and the relative Cartesian state has been developed. Expressions for the time-variation of ROEs, in terms of both relative Cartesian state parameters and initial ROEs, have been derived. Additional useful parameters related to ROEs have been defined.

Utilizing the ROE parameters, categories of relative motion can be visualized based upon three modes, depending upon values for three particular ROEs: the radial coordinate of the instantaneous center of motion, semimajor axis of the instantaneous relative ellipse, and amplitude of the cross-track motion. By superposing the modes, the behavior of the free-drift trajectory can be determined.

Acknowledgments The authors wish to acknowledge the following individuals who contributed to the development of the relative orbital element formulation: Steve Tragesser, Department of Aerospace Engineering, University of Colorado at Colorado Springs; Kenny Horneman, Barron Associates, Inc.; and Mark Tollefson, retired. The authors also acknowledge the United States Air Force Office of Scientific Research/Air Force Research Laboratory for their support of this work.

References

1. Woffinden, D.C., Geller, D., Mosher, T., Kwong, J.: On-orbit satellite rendezvous inspection: a concept study and design. *Spaceflight Mechanics 2005*. *Adv. Astronaut. Sci.* **120**(Parts 1 & 2), 849–867 (2005)
2. Sabol, C., Burns, R., McLaughlin, C.A.: Satellite formation flying design and evolution. *J. Spacecr. Rocket.* **38**(2), 270–278 (2001)
3. Fasano, G., D’Errico, M.: Design of satellite formations for interferometric and bistatic SAR. Institute of Electrical and Electronics Engineers Aerospace Conference Paper No. 1064. Mar. 2007
4. Carreau, M.: NASA Approves Orbital Sciences for ISS Commercial Resupply Missions. *Aviation Week and Space Technology*. October 1, 2013
5. Clark, S.: Satellite In-Space Servicing Demo Mission a Success. *Spaceflight Now*. July 23, 2007
6. Malik, T.: Prototype Satellites Demonstrate In-Orbit Refueling. Space.com. April 4, 2007
7. Air Force Space Command: Resiliency and Disaggregated Space Architectures. White Paper, AFD-130821-034. August 21, 2013
8. Pawlikowski, E., Loverro, D., Cristler, T.: Space: Disruptive Challenges, New Opportunities, and New Strategies. *Strateg. Stud. Q.* **6**, (1), Spring (2012)
9. Jezewski, D.J., Brazzell, J.P., Prust, E.E., Brown, B.G., Mulder, T.A., Wissinger, D.B.: A Survey of Rendezvous Trajectory Planning. *American Astronautical Society Paper*, pp. 91–505. Aug. 1991
10. Gaylor, D.E., Barbee, B.W.: Algorithms for safe spacecraft proximity operations. In: *Conference Proceedings, Space Flight Mechanics 2007, Advances in the Astronautical Sciences*, vol. 127, pp. 133–152 (2007)

11. Holzinger, M., DiMatteo, J., Schwartz, J., Milam, M.: Passively Safe Receding Horizon Control for Satellite Proximity Operations. In: Proceedings of the 47th IEEE Conference on Decision and Control, Cancun, Mexico, Dec. 2008
12. Breger, L., How, J.P.: Safe trajectories for autonomous rendezvous of spacecraft. *J. Guid. Control. Dyn.* **31**(5), 1478–1489 (2008)
13. Roger, A.B., McInnes, C.R.: Safety constrained free-flyer path planning at the international space station. *J. Guid. Control. Dyn.* **23**(6), 971–979 (2000)
14. Hill, G.W.: Researches in the lunar theory. *Am. J. Math.* **1**(1), 5–26 (1878)
15. Tschauner, J., Hempel, P.: Rendezvous zu einem in elliptischer Bahn umlaufenden Ziel. *Astronautica Acta* **11**(2), 104–109 (1965)
16. Clohessy, W.H., Wiltshire, R.S.: Terminal guidance system for satellite rendezvous. *J. Aerosp. Sci.* **27**(9), 653–658 (1960)
17. Condurache, D., Martinuși, V.: Relative spacecraft motion in a central force field. *J. Guid. Control. Dyn.* **30**(3), 873–876 (2007). Engineering Notes
18. Schaub, H., Junkins, J.L.: Analytical Mechanics of Space Systems, AIAA, Reston, Virginia (2003)
19. Vallado, D.A. Fundamentals of Astrodynamics and Applications, 2nd. Microcosm Press, El Segundo, California (2004)
20. Kaplan, M.H.: Modern Spacecraft Dynamics & Control. John Wiley and Sons, New York (1976)
21. Gustafson, D.E., Kriegsmann, B.A.: A guidance and navigation system for automatic stationkeeping in earth orbit. *J. Spacecr. Rocket.* **10**(6), 369–376 (1973)
22. Vaddi, S.S., Alfriend, K.T., Vadali, S.R., Sengupta, P.: Formation establishment and reconfiguration using impulsive control. *J. Guid. Control. Dyn.* **28**(2), 262–268 (2005)
23. D'Amico, S., Montenbruck, O.: Proximity operations of formation-flying spacecraft using an eccentricity/inclination vector separation. *J. Guid. Control. Dyn.* **29**(3), 554–563 (2006)
24. D'Amico, S.: Relative Orbital Elements as Integration Constants of Hill's Equations, DLR TN 05-08, December 15, (2005)
25. Gill, E., Montenbruck, O., D'Amico, S.: Autonomous formation flying for the PRISMA mission. *J. Spacecr. Rocket.* **44**(3), 671–681 (2007)
26. D'Amico, S., Ardaens, J.-S., Gaias, G., Benninghoff, H., Schlepp, B., Jørgensen, J.L.: Noncooperative rendezvous using angles-only optical navigation: system design and flight results. *J. Guid. Control. Dyn.* **36**(6), 1576–1595 (2013)
27. Han, C., Yin, J.: Formation design in elliptical orbit using relative orbital elements. *Acta Astronautica*, **77**. Aug.-Sept. 2012
28. Lovell, T.A., Tragesser, S.G.: Guidance for relative motion of low earth orbit spacecraft based on relative orbit elements. AIAA Paper. 2004–4988. Aug. 2004
D
29. Lovell, T.A., Tragesser, S.G., Tollefson, M.V.: A practical guidance methodology for relative motion of LEO spacecraft based on the clohessy-wiltshire equations. *Am. Astronaut. Soc. Pap.*, 04–252 (2004)
30. Bevilacqua, R., Lovell, T.A.: Analytical guidance for spacecraft relative motion under constant thrust using relative orbit elements. *Acta Astronautica* **102**, 47–61. September-October 2014
31. Phillips, M.: Spacecraft Collision Probability Estimation for Rendezvous and Proximity Operations. Master of Science Thesis, Utah State University, Logan Utah (2012)
32. Aubin, B.S.: Optimization of Relative Orbit Transfers Via Particle Swarm and Primer Vector Theory. Master of Science Thesis, University of Illinois at Urbana-Champaign (2011)
33. Schwartz, J., Krenzke, T., Hur-Diaz, S., Ruschmann, M., Schmidt, J.: Error-Contracting Impulse Controller for Satellite Cluster Flight Formation. Paper AIAA 2013-4541, presented at the AIAA Guidance, Navigation, and Control Conference, Boston, MA. 19–22 August 2013
34. Schwartz, J., Krenzke, T., Hur-Diaz, S., Ruschmann, M., Schmidt, J.: The Flocking Controller: A Novel Cluster Control Strategy for Space Vehicles. Paper AIAA 2013-4543, presented at the AIAA Guidance, Navigation, and Control Conference, Boston, MA. 19–22 August 2013
35. Chait, S., Spencer, D.A.: Prox-1: Automated Trajectory Control for On-Orbit Inspection. In: AAS 14-066, 37th Annual American Astronautical Society Guidance and Control Conference. January, 2014